Chemical Geology 559 (2021) 119969

Contents lists available at ScienceDirect

Chemical Geology

journal homepage: www.elsevier.com/locate/chemgeo

Lithium and its isotopes behavior during incipient weathering of granite in the eastern Tibetan Plateau, China

Jun-Wen Zhang [a], Zhi-Qi Zhao [b,c,*], Ya-Ni Yan [b], Li-Feng Cui [a], Qi-Lian Wang [d], Jun-Lun Meng [d], Xiao-Dong Li [a], Cong-Qiang Liu [a,**]

[a] Institute of Surface-Earth System Science, School of Earth System Science, Tianjin University, Tianjin 300072, China
[b] School of Earth Science and Resources, Chang'an University, Xi'an 710054, China
[c] Key Laboratory of Western Mineral Resources and Geological Engineering, Ministry of Education, Chang'an University, Xi'an 710054, China
[d] State Key Laboratory of Environmental Geochemistry, Institute of Geochemistry, Chinese Academy of Sciences, Guiyang 550081, China

ARTICLE INFO

Editor: E.B Michael

Keywords:
Lithium isotopes
Granite
Chemical weathering
Primary minerals

ABSTRACT

Lithium (Li) isotopes have been shown to be fractionated significantly during chemical weathering of silicate rocks. However, previous research has mainly been focused on basalt weathering, whereas the behavior of Li isotopes during the weathering of granite remains unclear. The Li isotopic compositions in the saprolite profile developed on granite was analyzed, as well as several individual primary minerals (K-feldspar, plagioclase, quartz and biotite) in the parent granite. Lithium concentration and the isotopic compositions of the individual primary minerals appear to be heterogeneous. Biotite is rich in Li (369.4 mg/kg), but the Li concentration is very low in other minerals (1.3–11.3 mg/kg). Quartz has the highest δ^7Li value (+19.9‰); other minerals contain δ^7Li within a fairly narrow range (+5.8‰ to +9.0‰). The saprolite samples were mainly composed of primary minerals and were characterized by low weathering intensity (CIA = 52–60). Lithium was distinctly lost in the saprolites relative to parent granite. Meanwhile, δ^7Li values of saprolites were all lower than those of parent granites (−2.0‰ to +3.9‰ vs. +7.1‰, respectively), which systematically decreased with increasing weathering intensity. The mineralogical composition and $^{87}Sr/^{86}Sr$ ratio in the saprolites suggest that the biotite was preferentially weathered below 120 cm depth in the examined profile, whereas plagioclase weathering mainly occurred above 120 cm depth. The Li released during granite weathering was characteristically different from the isotopes in the primary minerals. Lithium isotopic fractionation during granite weathering is affected by adsorption and/or incorporation of Li by secondary minerals (or clay minerals), and the release of Li from biotite. This study highlights the fact that significant Li isotope fractionation occurs during Li leaching (relatively higher $^7Li/^6Li$ ratios) from biotite in the incipient stage of granite weathering, which may help to explain the higher δ^7Li values found in the dissolved load from the catchments of low weathering intensity.

1. Introduction

Chemical weathering of silicate rocks plays a critical role in the sequestration of atmospheric CO_2 through deposition of carbonates in the oceans, thereby regulating the Earth's climate on a geological time scale (e.g., Berner, 1990). The uplift of the Tibetan Plateau driving increases in chemical weathering may have resulted in decreases of atmospheric CO_2 concentration over the past 40 Ma (Raymo and Ruddiman, 1992). Furthermore, chemical weathering contributes significantly to the chemical composition of river waters, which further affects the evolution of seawater chemistry (Wallmann, 2001).

Previous studies have shown that lithium (Li) and its isotopes can provide information on continental silicate weathering (e.g., Pogge von Strandmann et al., 2020). Naturally, Li is hosted predominantly by silicate minerals, and relatively less so in carbonates, and thus more than 90% of dissolved Li is derived from silicates even in carbonate-dominated catchments (Huh et al., 1998, 2001; Kısakürek et al., 2005). The two stable isotopes (^{6}Li and ^{7}Li) of Li have a large mass difference (~16%), resulting in a correspondingly large mass-dependent fractionation potential in low-temperature water-rock reactions. Studies

* Corresponding author at: School of Earth Science and Resources, Chang'an University, Xi'an 710054, China.
** Corresponding author.
E-mail addresses: zhaozhiqi@chd.edu.cn (Z.-Q. Zhao), liucongqiang@tju.edu.cn (C.-Q. Liu).

https://doi.org/10.1016/j.chemgeo.2020.119969
Received 22 April 2020; Received in revised form 14 September 2020; Accepted 25 October 2020
Available online 28 October 2020

of Li isotopes in weathering profiles and/or soils developed on basalts (or other igneous rocks) have shown significant differences between the δ^7Li values in weathered products and parent rocks, attributed to preferential incorporation of ^{6}Li into newly formed secondary minerals (such as clays, zeolites, and oxyhydroxides) during weathering (e.g., Wimpenny et al., 2010a; Liu et al., 2013; Hindshaw et al., 2019). As a result, weathered products (δ^7Li = −20‰ to +3.0‰) are generally isotopically lighter than the parent rocks (−4.3‰ to +6.0‰) (Kısakürek et al., 2004; Rudnick et al., 2004; Liu et al., 2013), mid-ocean ridge basalts (+3.5 ± 1.0‰, 2σ) and upper continental crust (UCC) (+0.6 ± 0.6‰, 2σ) (Sauzéat et al., 2015; Marschall et al., 2017), and correspond to the isotopically heavier Li found in the dissolved load in rivers (+2.1‰ to +43.7‰) (Huh et al., 2001; Kısakürek et al., 2005; Dellinger et al., 2015; Wang et al., 2015; Pogge von Strandmann et al., 2017; Gou et al., 2019; Murphy et al., 2019; Ma et al., 2020).

It is generally believed that (1) during the incipient stage of weathering and in catchments of low chemical weathering intensity, the congruent weathering process (a high ratio of primary rock dissolution relative to secondary mineral formation (Pogge von Strandmann et al., 2017)) cannot result in significant Li isotope fractionation, and the δ^7Li values of weathering products and dissolved load in rivers are close to those in primary rock; and (2) more incongruent weathering shows remarkable Li isotope fractionation due to the formation of large amounts of secondary minerals (e.g., clays), resulting in isotopically lighter Li in weathered products and heavier Li in dissolved loads (Pistiner and Henderson, 2003; Ryu et al., 2014; Pogge von Strandmann and Henderson, 2015; Pogge von Strandmann et al., 2017; Maffre et al., 2020). However, significant Li isotope fractionation has also been observed in incipient weathering catchments with the bedrocks characterized by phaneritic rocks (e.g., granite), which has been attributed to adsorption of ^{6}Li by newly formed Fe/Mn-oxyhydroxides (Huh et al., 2001; Millot et al., 2010; Wimpenny et al., 2010a). Thus, there seems to be a different Li isotope fractionation characteristic between the chemical weathering of phaneritic and aphanitic rocks.

Granite is a phaneritic rock comprising several different primary minerals, including quartz, feldspars and mica. The concentrations of Li and its isotope composition are very heterogeneous in granite. For example, Li is enriched in biotite while quartz contains the relatively isotopically heavier Li (Teng et al., 2009; Sun et al., 2016; Li et al., 2018). Pistiner and Henderson (2003) found that δ^7Li value in the solution of partially dissolved granite was about 7.4‰ lighter than that of whole-rock values, which they attributed to the δ^7Li differences in the primary minerals and secondary minerals. Studies of Li isotope composition in granitic weathering products indicate that the formation of secondary minerals and non-congruent dissolution of parent rock are the main reasons for Li isotope fractionation during weathering of granite (Rudnick et al., 2004; Lemarchand et al., 2010; Négrel and Millot, 2019). To sum up, two processes may lead to Li isotope fractionation during granite weathering. First, similar to previous opinions, ^{6}Li may be preferentially incorporated into newly formed secondary minerals; second, due to the primary minerals of granite may have different Li concentration and isotopic composition, the process of differential weathering of primary minerals (successive weathering of biotite, plagioclase and K-feldspar) releases Li may also lead to the variation in δ^7Li value in the weathering products. Additionally, externally-derived Li (e.g., from marine aerosol or eolian dust) also affect the δ^7Li values in the top layer of the weathering profile (Pistiner and Henderson, 2003; Huh et al., 2004; Kısakürek et al., 2004; Liu et al., 2013; Li et al., 2020). Very few previous studies on Li isotope behavior during granite weathering have been reported (Rudnick et al., 2004; Lemarchand et al., 2010; Négrel and Millot, 2019).

Thus, the aim of this study is to improve our understanding of Li isotope behavior during granite weathering. The primary mineral weathering layer was carefully delineated in a saprolite profile based on mineralogical composition, as well as the presence of major and trace elements and Sr isotopes in the saprolites and the parent granite. The prevalence of Li isotopes in the primary minerals (K-feldspar, plagioclase, quartz and biotite) separated from the granite were analyzed. Potential controlling factors of Li isotope fractionation during the incipient stage of granite weathering are discussed, for example, the formation of secondary minerals and the differential weathering of primary minerals.

2. Sampling

A saprolite profile with low weathering intensity developed on granite was collected in June 2016 on the eastern Tibetan Plateau, China (mean annual temperature ~ 4 °C; mean annual precipitation ~600 mm) (Fig. 1). The sampling site was located on the side of a mountain about 3758 m above sea level. This is a granitic pluton with a U—Pb age of 216 Ma derived from partial melting of late Paleoproterozoic to early Mesoproterozoic mafic–intermediate lower crust containing < 20% added depleted mantle-derived magma (He et al., 2013).

Saprolite samples were collected from the top of the parent granite from the surface to a depth of about 180 cm. The samples were collected from the surface to 100 cm depth in a 5 cm layers, then eight further saprolite samples were collected below 100 cm, each with a layer thickness of 10 cm. Each sample contained about 2 kg saprolite. Two samples of the parent granite (~2 kg for each one, ~15 × 8 × 8 cm^3) were collected at the same site. The weathering intensity of the saprolite at this site is relatively low; the profile consists mainly of coarse grains up to ~5 mm diameter, without any obvious soil layer. Furthermore, the weakly altered granite close to the bottom of the sampled profile preserves the texture of the parent rock without obvious layering, and preserves the structures of partial primary minerals.

3. Analytical methods

The saprolite samples were homogenized in the laboratory after air drying, and then ~50 g of each sample was transferred into an agate mill and ground to below 74 μm passed through a nylon sieve. The samples from the upper 40 cm were not analyzed due to the presence of a clear discontinuity at this depth, indicating the likelihood that above this depth the materials had been transported and were not products of in situ weathering. The granites samples were crushed to smaller than 2 mm before grinding. For the samples of individual primary minerals, the parent rock was crushed to particle a size between 250 and 380 μm, then pure mineral samples of plagioclase, K-feldspar, quartz and biotite were selected under a stereo microscope. The sample powder was analyzed to determine the mineralogical composition, major and trace elements, and Li, Sr and Nd isotopes.

Major elements and mineralogical composition were analyzed by X-ray fluorescence (XRF) and X-ray diffraction (XRD) at the State Key Laboratory of Biogeology and Environmental Geology, China University of Geosciences, Wuhan. Trace elements were determined by inductively coupled plasma mass spectrometry (ICP-MS) at the State Key Laboratory of Environmental Geochemistry, Institute of Geochemistry, Chinese Academy of Sciences. The Fe, Mg, and Ti concentrations in the individual primary minerals were analyzed using inductively coupled plasma optical emission spectrometry (ICP-OES) after digestion. XRD analysis gave an estimated mineral percentage in each sample. Chinese national standard samples GBW07105 (basalt) and GBW07109 (syenite) were used to calibrate the instrument for major element determination. USGS standards AGV-2 and GSP-2 were further used as controls to ensure the accuracy of trace element determination. Precision for most major and trace elements was better than ± 5% (2σ) and ± 10% (2σ), respectively.

Lithium isotope analysis was based on the method described by Wang et al. (2015), slightly modified in this study. Briefly, ~50 mg of sample powder was dissolved in 3 mL of concentrated HF and HNO_3 (3:1, v/v) in Savillex screw-top beakers on a hot plate (120 °C, 48 h), followed by successive refluxing with concentrated HNO_3 and HCl. The

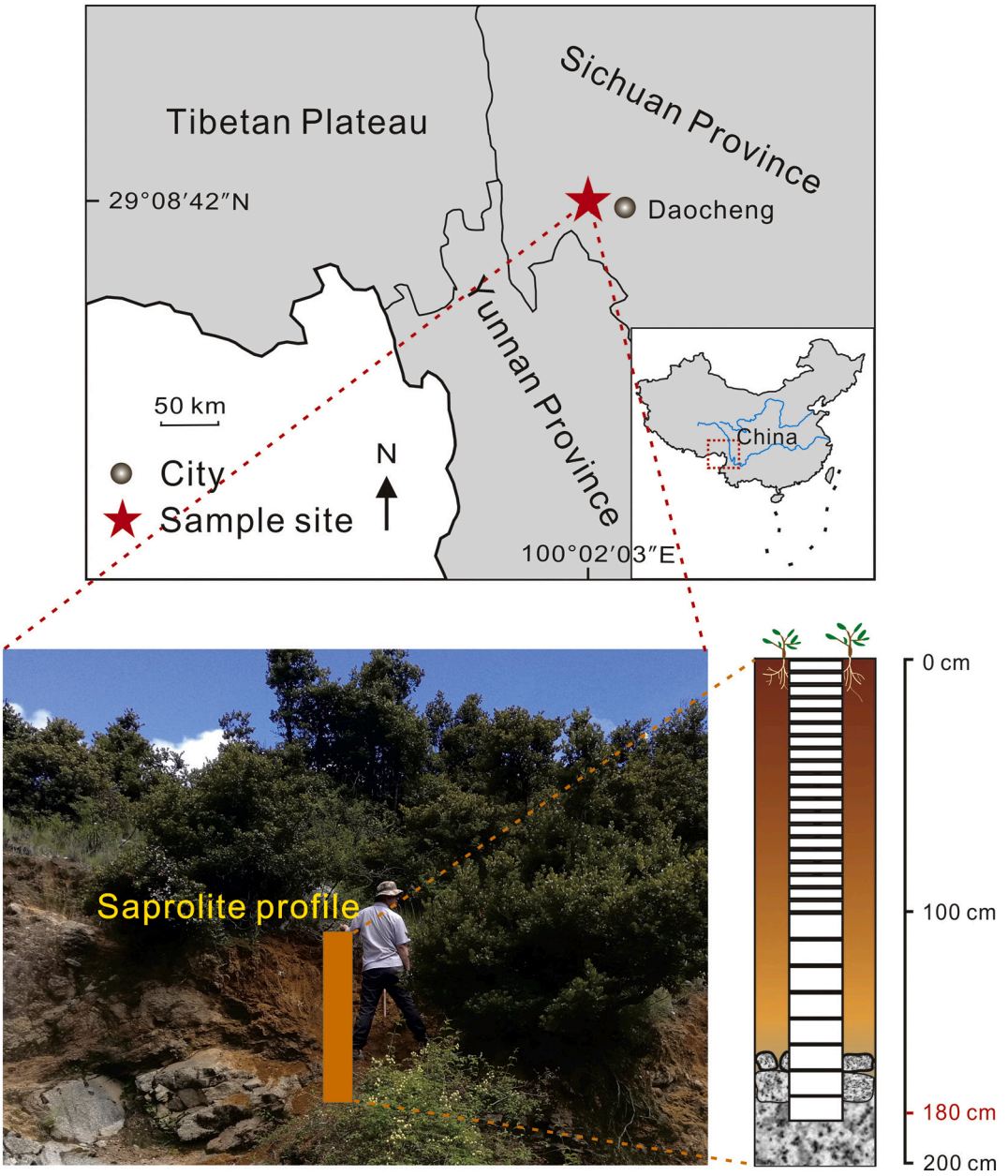

Fig. 1. Map of the sampling site.

final solution was dissolved in 1 mL of 0.40 M HCl. Lithium was purified in a cation exchange column (Bio-Rad AG 50 W-X12 resin, 200–400 mesh) and eluted with 0.40 M HCl. Purification was duplicated to ensure a relatively pure Li solution. The eluted solution containing Li was evaporated to dryness on a hot plate (120 °C) and re-dissolved in 2% HNO_3. The Li content of the partial solutions was determined and the calculated Li recovery rate of the samples was between 98.1% and 103.6% (Zhang et al., 2019). Ultra-pure water (18.2 MΩ·cm) was prepared using a Milli-Q IQ Element system (Merck, USA). A stock of concentrated HF, HNO_3 and HCl was acquired using a DST-1000 acid purification system (Savillex, USA). Lithium isotope ratios were determined by multi-collector ICP-MS (Nu Plasma II, Wales, UK), using the sample standard bracketing (SSB) method. International standard L-SVEC (NIST RM 8545) with similar Li concentration to the samples (~80 ng/mL) was used in this study. The external precision (2σ) of this technique, obtained by repeated dissolution, purification and analysis of seawater and rock standard samples, is < ±0.8‰. The measured δ^7Li values of seawater and the rock standards AGV-2 and GSP-2 were + 31.4 ± 0.7‰ (n = 18), +7.23 ± 0.16‰ (n = 4) and − 0.10 ± 0.18‰ (n = 4) (Table S1), respectively, in good agreement with previously published values (Choi et al., 2013; Lin et al., 2016; Pogge von Strandmann et al., 2017).

The $^{87}Sr/^{86}Sr$ ratio was determined by multi-collector ICP-MS (Nu Plasma II) after separation through a cation exchange column (Bio-Rad AG 50 W-X8 resin, 200–400 mesh) and eluted with 2.0 M HNO_3. The reproducibility of the measurement was checked by analysis of the NBS 987 standard, which yielded a mean $^{87}Sr/^{86}Sr$ of 0.710238 ± 11 (2σ, n = 11). The procedure for separating Nd from the saprolite and granite samples used a standard ion chromatography column as described by Che et al. (2018). The $^{143}Nd/^{144}Nd$ ratio was determined by multi-collector ICP-MS (Neptune Plus) and the reproducibility was checked by comparison with the JNdi-1 standard, which yielded a mean $^{143}Nd/^{144}Nd$ of 0.512094 ± 10 (2σ, n = 12). The measured $^{87}Sr/^{86}Sr$ and $^{143}Nd/^{144}Nd$ ratios for the rock standard GSP-2 were 0.764948 ± 8 (2σ, n = 2) and 0.511362 ± 7 (2σ, n = 2), respectively, which were comparable with the values of 0.764962 ± 4 (2σ) and 0.511353 ± 4 (2σ) of

the materials from previous studies (Raczek et al., 2003 and references there in).

4. Results

4.1. Mineralogy

The XRD analysis suggested that the saprolite and parent granite were mainly composed of the primary minerals quartz, plagioclase and K-feldspar (Fig. 2 and Fig. S1). Biotite was abundant in the parent granite (up to ~10%), but its abundance decreased systematically to generally <1% in the saprolite towards the surface above 120 cm depth. Conversely, the percentages of chlorite and vermiculite in the saprolite gradually increased towards the surface from 1% to 27% and < 1% to 13%, respectively, then decreased to about 10% and 8%, respectively near the surface.

4.2. Major and trace elements

Concentrations of major and trace elements in the saprolite and parent granite are listed in Table S2. The saprolites were mainly composed of silicon (SiO_2, average 70.5%) and aluminum (Al_2O_3, average 15.6%), followed by potassium (K_2O, average 4.5%) and sodium (Na_2O, average 3.3%). The Fe and Mg contents showed similar trends, with both decreasing in the profile between 80 cm and 180 cm depths, and vice versa between 120 cm and 80 cm depths (Fig. 3B). However, between 80 cm and 40 cm, contents of Mg declined towards the surface, while Fe content remained relatively constant.

The weathering intensity was indicated by the chemical index of alteration (CIA), defined as the molar ratio of $Al_2O_3/(Al_2O_3 + CaO^* + Na_2O + K_2O) \times 100$, where CaO* represents Ca that is not present in carbonates and phosphates (Nesbitt and Young, 1982). In the present work, Ca from apatite was corrected by the P_2O_5 content, and Ca from carbonate was not corrected because little carbonate was present in the saprolites, as indicated by Ca/Na < 1in the samples (e.g., Rudnick et al., 2004). The CIA value of the parent granite is 51.4, which lies within the range 45–55 for fresh granites (Nesbitt and Young, 1982). Slightly higher than that of parent granite, the CIA values of the saprolite samples increased from 52 to 60 towards the surface (Fig. 3A). The low CIA values of the saprolite profile confirmed the relatively low weathering intensity.

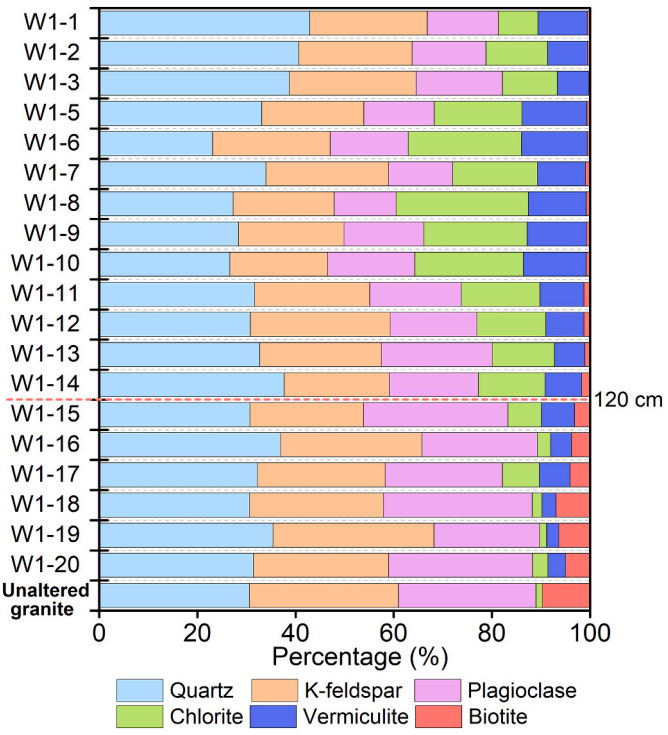

Fig. 2. Composition of mineral phases in saprolites and parent granite.

The refractory elements, such as Nb, Ta, Zr, Hf, and Ti, are generally considered to be relatively immobile during weathering (e.g., Middelburg et al., 1988), which is useful for quantitatively evaluating the relative depletion or enrichment of the mobile elements such as Na and Li. The parameter tau [$\tau_j = (C_{j,w} \times C_{i,p})/C_{j,p} \times C_{i,w})$-1] defines the relative gain ($\tau_j > 0$) or loss ($\tau_j < 0$) of elements during weathering, where C is the concentration of the mobile (j) or immobile (i) elements in weathered (w) or parent (p) materials (Chadwick et al., 1990). In this study, Zr was adopted as the immobile element to calculate the tau values (more details can be found in the supplementary materials) (Fig. S2).

4.3. Li concentration and isotopic composition

Nine fresh granite samples from different areas in China were analyzed for Li concentrations ([Li]) and δ^7Li values (Liu et al., 2016; Mao et al., 2018). [Li] and δ^7Li varied from 21.0 to 58.6 mg/kg (mean 38.5 mg/kg) and from −1.4‰ to +7.4‰ (mean + 1.7‰), respectively. These values fall within the ranges reported for granites in other areas ([Li] and δ^7Li ranging from 4.7 to 661 mg/kg and from −1.9‰ to +9.0‰, respectively) (Romer et al., 2014; Sun et al., 2016; Li et al., 2018), and are also close to the statistical mean values of 33 ± 32 mg/kg (1σ, n = 188) and 2.0 ± 2.3‰ (1σ, n = 130) reported by Teng et al. (2009) for granites worldwide.

Lithium concentration and δ^7Li in individual primary mineral samples (K-feldspar, plagioclase, biotite and quartz) were analyzed (Fig. 4). Twenty-eight mineral samples were separated from the nine granites described above. The results show that Li is mainly hosted in biotite (201.4–1206 mg/kg, mean 448.2 mg/kg), with relatively low [Li] in quartz (3.6–22.1 mg/kg, mean 14.4 mg/kg), plagioclase (3.5–18.6 mg/kg; mean 6.8 mg/kg) and K-feldspar (1.3–6.8 mg/kg; mean 3.9 mg/kg). The distributions of Li in these minerals are similar to those reported in previous studies (Sun et al., 2016; Li et al., 2018). The variations of δ^7Li in K-feldspar (−1.4‰ to +9.0‰, mean + 4.3‰), plagioclase (−1.6‰ to +5.9‰, mean + 1.1‰) and biotite (−0.7‰ to 5.8‰, mean + 1.7‰) were similar. The quartz had the highest δ^7Li value (+12.9‰ to + 21.8‰, mean + 17.6‰), consistent with data reported for minerals from pegmatite and other granites (Teng et al., 2006a; Sun et al., 2016; Li et al., 2018; Négrel and Millot, 2019).

The concentration of Li in the saprolites varied between 22.7 and 69.8 mg/kg. The vertical profile of Li was similar to that of Fe and Mg (Fig. 3B). The calculated τ_{Li} values for the saprolites were all less than 0 (−64% to −7.7%, mean −40%) and decreased gradually upwards from 120 cm depth towards the surface. However, the τ_{Li} values showed an increasing trend towards the surface from 120 cm depth. This observation is similar to the increase in τ_{Li} values in the top saprolite layer of other silicate weathering profiles (Kısakürek et al., 2004; Liu et al., 2013). The weathered products were distinctly isotopically lighter than the parent granites (+7.1‰). Sprolite δ^7Li varied from +3.9‰ near the interface with the +7.1‰ (parent granite) to +0.5‰ at 120 cm depth. Above this level saprolite δ^7Li ranged from −2.0 to +0.9‰ (Fig. 5B). These results are consistent with previous study results that indicated that the weathered products are isotopically lighter than the parent granites (Rudnick et al., 2004; Négrel and Millot, 2019).

4.4. Sr concentration and isotopic composition

Strontium was mainly hosted in plagioclase (80.9–615 mg/kg, mean 290 mg/kg) and K-feldspar (42.8–709 mg/kg, mean 202 mg/kg), with lower concentrations in biotite (4.3–44.2 mg/kg, mean 14.9 mg/kg). The $^{87}Sr/^{86}Sr$ ratio in the K-feldspar (0.73526) was slightly higher than

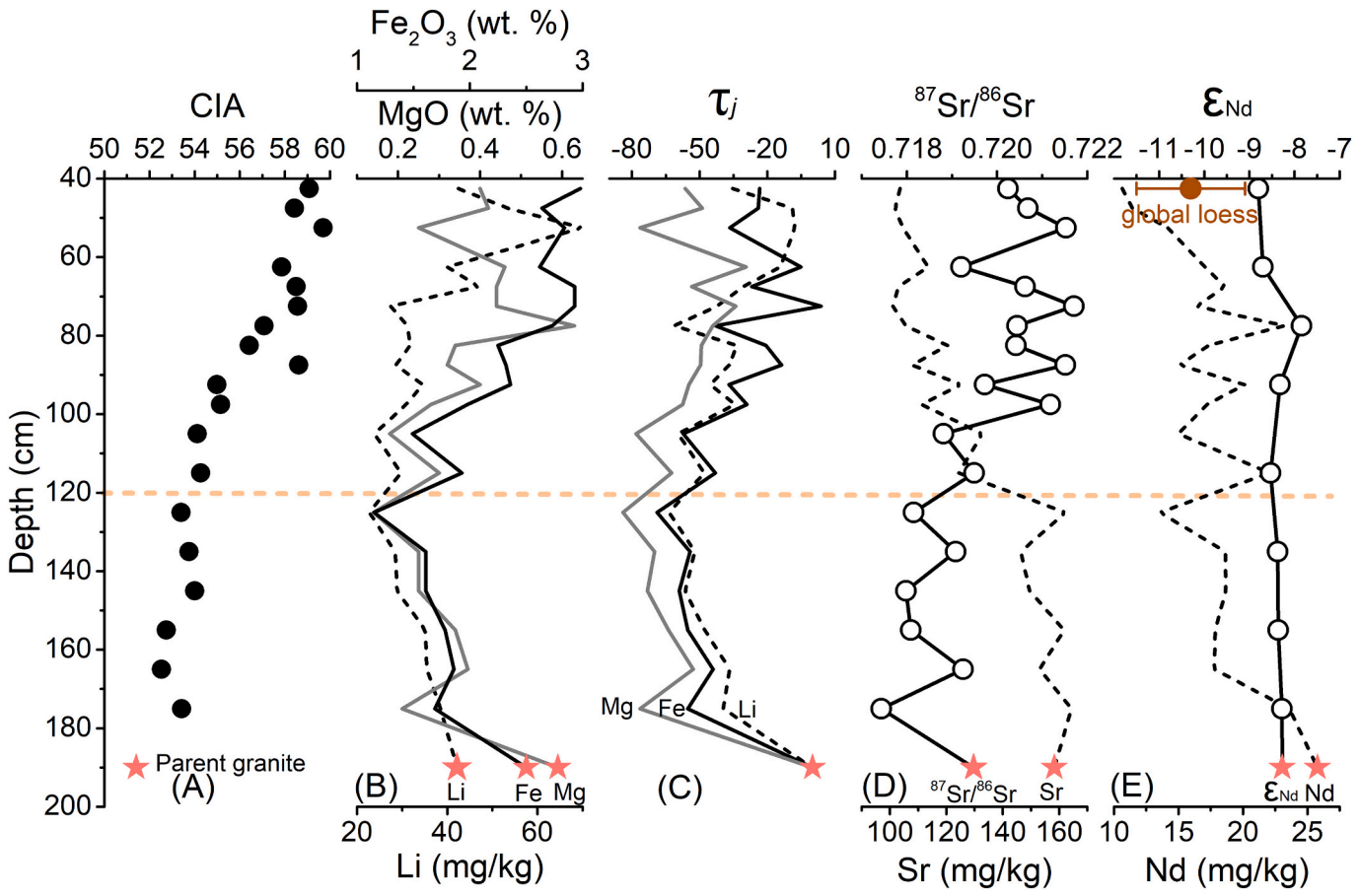

Fig. 3. Depth profile of CIA, τ values, Fe, Mg, Li, Sr, Nd, $^{87}Sr/^{86}Sr$ ratios and ε_{Nd}. The ε_{Nd} value of loess (global loess samples) from Chauvel et al. (2014).

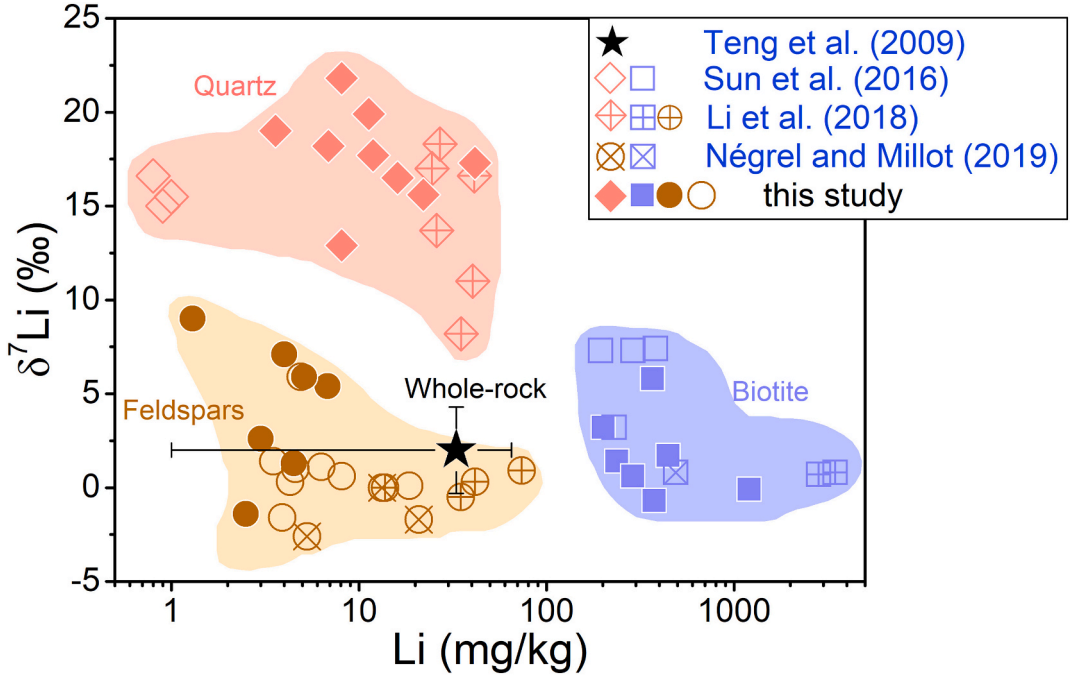

Fig. 4. Plot of δ^7Li vs. [Li] (mg/kg) in individual primary minerals separated from different granites and whole-rock granite. The star represents the whole rock. Brown solid circles = K-feldspar; hollow circles = plagioclase; diamonds = quartz; squares = biotite.

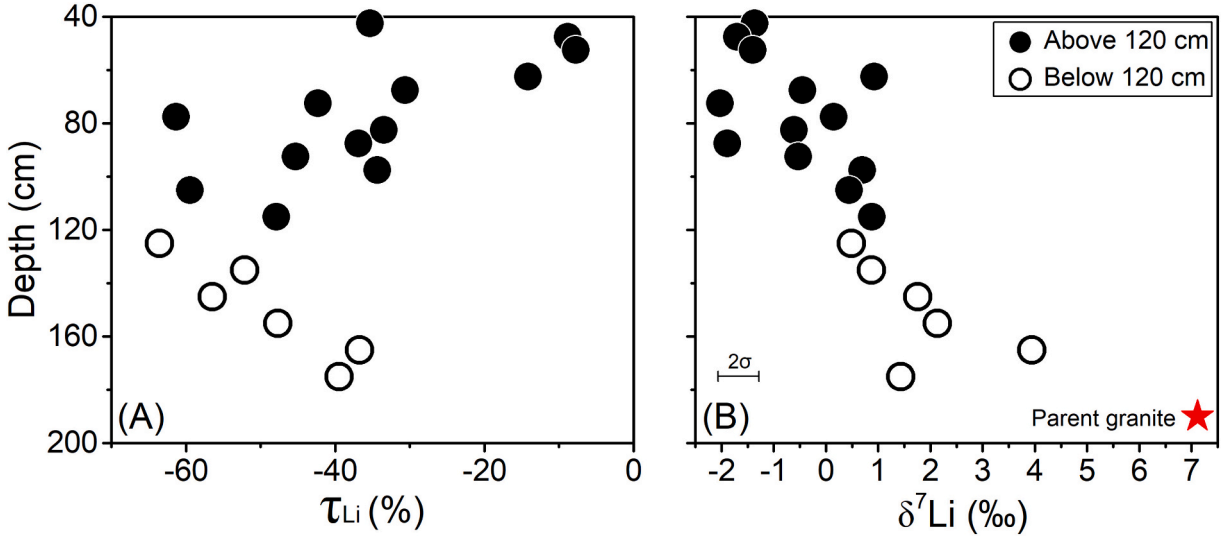

Fig. 5. Depth profile of τ_{Li} and δ^7Li.

Table 1
Element concentrations and Li and Sr isotopic composition in individual primary minerals.

	Fe (g/kg)	Mg (g/kg)	Ti (g/kg)	Nb (mg/kg)	Ta (mg/kg)	Zr (mg/kg)	Hf (mg/kg)	Sr (mg/kg)	Li (mg/kg)	$^{87}Sr/^{86}Sr$	$^{87}Sr/^{86}Sr^b$	δ^7Li (‰)
Plagioclase	0.38	<0.01	0.03	0.41	0.14	3.19	0.13	267.2	4.9	0.71147	0.7083	+5.9
K-feldspar	0.15	<0.01	0.02	0.11	0.04	3.71	0.14	162.6	1.3	0.73526	0.7160	+9.0
Quartz	0.03	0.02	0.03	0.64	0.07	4.71	0.15	1.5	11.3	nd[a]		+19.9
Biotite	92.1	26.0	11.0	113.6	13.5	46.7	1.3	4.3	369.4	nd	1.1060	+5.8

[a] nd = not determined; data of $^{87}Sr/^{86}Sr^b$ from White et al. (2001).

that in the plagioclase (0.71147), in agreement with data reported by White et al. (2001) (Table 1). The $^{87}Sr/^{86}Sr$ ratio in biotite was not measured in this study. However, data from previous studies suggest that $^{87}Sr/^{86}Sr$ ratio in biotite (e.g., 1.1060 and 1.1312) is generally significantly higher than that in K-feldspar and plagioclase of the same granite sample (Blum and Erel, 1997; White et al., 2001).

For the weathering products, below 120 cm depth, a narrow range of Sr concentrations in saprolites was observed (146.4–164.4 mg/kg, mean 156.2 mg/kg), which was slightly lower than that of parent granite (158.3 mg/kg). The $^{87}Sr/^{86}Sr$ ratios in the saprolites (0.71744–0.71925, mean 0.71833) were also slightly lower than in the parent granite (0.71948). Above 120 cm depth, the Sr concentrations in the saprolites decreased gradually with the minimum (~100 mg/kg) appearing near the surface. Conversely, the $^{87}Sr/^{86}Sr$ ratios of the saprolites were generally higher than that of parent granite and increased towards the surface (maximum 0.72153) (Fig. 3D). The $^{87}Sr/^{86}Sr$ of the saprolites showed an undulating trend with an initial decrease and then increases, which is consistent with the reported results of previous studies of granite weathering profiles (Ma and Liu, 2001; White et al., 2001).

4.5. Nd concentration and isotopic composition

The concentration of Nd in the saprolites was lower than that of parent granite, and showed a decreasing trend towards the surface of the profile (Fig. 3E). The $^{143}Nd/^{144}Nd$ ratio of the parent granite was 0.512213, which is within the range of 0.512146 to 0.512230 in granites collected from the study area previously (He et al., 2013). The $^{143}Nd/^{144}Nd$ ratio of the saprolites (0.512187–0.512236, mean 0.512208) is almost identical to that of parent granite and is relatively constant in the weathering profile (Fig. 3E). Additionally, the calculated ε_{Nd} values of the saprolites (−8.4 ± 0.3 (1σ)) were higher than the average for the UCC (−10.3 ± 1.2, 1σ) and for Chinese loess (−10.3 ± 1.6 (1σ) (Yokoo et al., 2004; Chauvel et al., 2014).

5. Discussion

5.1. Factors affecting Li mobility during weathering of granite

Lithium is generally leached during weathering because it is a fluid-mobile element, similar to Ca, Na and K (Rudnick et al., 2004). Below 120 cm depth of the profile, Li has been gradually leached (minimum τ_{Li} = −64%) as the weathering progressed. However, above 120 cm depth, the loss of Li by leaching decreases upwards in the profile. Potential factors affecting Li mobility during weathering of granite (e.g., loss of Li by decomposition of primary minerals) and re-adsorption of Li by formation of secondary minerals (such as clays and Fe-oxyhydroxide) are discussed below. In addition, the effect of externally-derived Li on the Li content in the top layer of the profile is also evaluated in this study.

5.1.1. Differential weathering of primary minerals

Since the concentration of Li in the primary minerals biotite, feldspars, and quartz varies by factors of tens to hundreds, the sequential decomposition of primary minerals significantly affects Li mobility during the weathering of granite. Generally, dark minerals (amphibole and biotite) are preferentially weathered, followed by plagioclase, K-feldspar, muscovite and quartz (e.g., Ma and Liu, 2001).

In this study, K-feldspar and quartz were not significantly weathered in the saprolites due to the low weathering intensity in the profile being examined (Liu et al., 2016). Biotite weathering was predominant at the incipient stage of weathering (i.e., below 120 cm depth), followed by the weathering of plagioclase (above 120 cm depth). This can be seen from the mineralogical composition of saprolites in the profile. The content of biotite decreased gradually towards the surface, and was almost depleted above 120 cm, while the plagioclase content was relatively stable below 120 cm depth, then decreased obviously towards the surface afterwards (Fig. 2). On the other hand, the sequential weathering of primary minerals was also confirmed by the Sr concentration and

isotopic composition variations in the weathering profile (White et al., 2001). Relative to feldspars, the biotite had a low Sr concentration but a very high $^{87}Sr/^{86}Sr$ ratio (Table 1). Below 120 cm depth, the Sr concentration and $^{87}Sr/^{86}Sr$ ratio in the saprolites were both slightly lower than those in the parent granite, showing a roughly decreasing trend towards the surface (Fig. 3D). This suggests that the preferential weathering of biotite released Sr with a high $^{87}Sr/^{86}Sr$ ratio at this stage. In contrast, above 120 cm depth, Sr was lost significantly, whereas $^{87}Sr/^{86}Sr$ ratio showed an increasing trend towards the surface. The rapid weathering of plagioclase was indicated by its high Sr concentration and low $^{87}Sr/^{86}Sr$ ratio. This observation agrees well with previous estimations that biotite weathers approximately eight times faster than plagioclase in the youngest soil profile (Blum and Erel, 1997). It is also consistent with previous observation that successive weathering of biotite, plagioclase and K-feldspar occurs during granite weathering (Ma and Liu, 2001), however, no significant K-feldspar weathering process was observed in the studied profile, most likely due to the low weathering intensity (CIA<60).

Because of the abundance of Li in biotite, a large proportion is lost during the weathering of biotite. As expected, during early stage weathering of granite below 120 cm depth, τ_{Li} values substantially decreased towards the surface (from 0 to −64%). Additionally, a good positive relationship was found between τ_{Li} and biotite content (R^2 = 0.85, not shown) in the saprolites below 120 cm depth, suggesting that Li was significantly lost during weathering of biotite. Moreover, biotite also contains an abundance of Fe, Mg, Ti and Nb, which are also significantly leached during biotite weathering. Therefore, it is not surprising that the vertical weathering profiles of τ_j (j = Li, Fe, Mg, Ti, Nb, etc.) exhibited similar systematic upward decreases below 120 cm depth (Fig. 3C and Fig. S2). However, above 120 cm depth (Fig. 2), it was found that the concentration of Li, Fe, Mg, etc. in the saprolite unexpectedly increased towards the surface (Fig. 3B). It was considered that this observation was possibly due to the rapid depletion of Ca and Na along with the weathering of plagioclase, resulting in the relative enrichment of Li, Mg and Fe. Nevertheless, when these elements were normalized to Zr, the τ_j values still showed an increasing trend towards the surface (Fig. 3C), suggesting that the loss of Li decreased with increasing weathering intensity.

This counterintuitive observation led to the speculation that there are two possible causes: first, for un-explained reason(s), Li (and Fe, Mg, etc.) was not leached significantly above 120 cm depth; second, the input of externally-derived substances with high concentrations of Li (and Fe, Mg, etc.) resulted in the relative enrichment of these elements in the saprolites near the top layer (discussed below).

5.1.2. Redox conditions

Although Li is insensitive to redox conditions due to its single redox state (+1 charge), it is adsorbed on and/or coexists with Fe/Mn-bearing secondary minerals (e.g., oxyhydroxides) which are very sensitive to redox conditions. Previous studies have shown that Li can be adsorbed by Fe/Mn-oxyhydroxides phases, and up to ~65% of the Li is associated with Fe-oxyhydroxide phases in the river sediments (Chan and Hein, 2007; Wimpenny et al., 2010a). As the redox condition varies, the amount of Fe-bearing secondary minerals formed may affect the mobility of Li in the weathering profile. Therefore, the prevailing redox conditions may also play an important role on Li concentration in the saprolite samples. The position of the water table may affect the redox conditions of weathering profiles (Kısakürek et al., 2004; Rudnick et al., 2004). However, this scenario seems unlikely to occur in the study profile, because sampling site of the profile is located near the top of a mountain and significantly higher than the water table in the area.

Above 120 cm depth, the τ_{Fe} value shows an increasing trend towards the surface (Fig. 3C), suggesting that most of Fe is retained in the saprolite near the surface. This observation may be attributed to the oxidizing environment near the surface caused by the diffusion of atmospheric oxygen and infiltration of oxic rainwater. Under oxidation conditions, Fe^{2+} released from weathered minerals like biotite is immediately oxidized to Fe(III), resulting in the in situ formation of Fe-oxyhydroxides and the re-adsorption of the leached Li and Mg on these newly formed secondary minerals. Additionally, with higher retention of Li and Mg in secondary minerals (e.g., vermiculite, formed by altered biotite), it is quite possible that more Fe, Li and Mg are retained in the saprolite above 120 cm depth.

With the downward infiltration of oxic rainwater, the dissolved oxygen is consumed by reducing elements such as Fe(II) and Mn(II) and/or by microbial respiration or by plant roots. Below 120 cm depth, τ_{Fe} decreased as the depth increased, reaching a minimum value of −68.8% at 120 cm depth (Fig. 3C). It is speculated that oxygen was almost exhausted near the 120 cm depth and most of the released Fe^{2+} was not oxidized to Fe(III) below 120 cm depth, and was mobilized by the water flow. Correspondingly, much of Fe was lost as weathering progressed and fewer Fe-bearing secondary minerals were formed. Meanwhile, the Li, Mg, Ti and Nb content decreased as weathering progressed, reflected in the good positive correlations observed between τ_{Fe} and τ_j (j = Li, Mg, Ti and Nb) below 120 cm depth (Fig. S3). Therefore, it is concluded that the mobility of Li and other elements enriched in biotite (Mg, Ti, Nb, Ta, etc.) during granite weathering was significantly controlled by the amount of Fe-bearing secondary minerals formed, which is affected by the redox conditions.

5.1.3. Input of externally-derived Li

Previous studies have suggested that the input of eolian dust with high Li content may have led to the increase in Li concentration near the surface of the saprolite profile (Huh et al., 2004; Kısakürek et al., 2004; Liu et al., 2013). However, in the present case it is considered unlikely that externally-derived Li was responsible for the increase of Li concentration near the surface. The Nd isotope was used to trace the sources of materials, including eolian dust (e.g., Rao et al., 2008). As the Nd isotopic composition of the saprolites was almost identical to that of parent granite (Fig. 3E), no externally-derived Li input is confirmed. The ε_{Nd} values in the saprolites were clearly lower than that in the UCC as estimated from global loess samples, including and Chinese loess which is the potential source of externally-derived Li. This conclusion is also supported by the Li concentration of the saprolites near the surface (> 40 mg/kg) higher than that of the UCC (30.5 ± 3.6 (2σ) mg/kg) and Chinese loess (30.5 to 40 mg/kg) (Sauzéat et al., 2015).

5.2. Mechanisms of Li isotope fractionation

A number of previous studies have shown that the formation of secondary minerals associated with the dissolution of primary minerals is mainly responsible for Li isotope fractionation during the chemical weathering of silicate rocks (e.g., Ryu et al., 2014; Liu et al., 2013; Pogge von Strandmann et al., 2017). This is due to the preferential incorporation of ^6Li into the octahedral structures of newly formed secondary minerals, whereas ^7Li is preferentially leached in the liquid phase (Pistiner and Henderson, 2003; Hindshaw et al., 2019; Li and Liu, 2020). In the isotope fractionation process at equilibrium, the heavier isotope is preferentially partitioned into sites with the highest bond energy: for example, Li^+ forms tetrahedral coordination with four water molecules (Yamaji et al., 2001; Schauble, 2004). In the present profile, δ^7Li values tended to decrease as the content of secondary minerals increased (Fig. 6). Accordingly, Li isotope fractionation was related to the formation of more secondary minerals in the saprolites (e.g., chlorites and vermiculite) as weathering progressed. Certainly, with the exception of smectite, many secondary (or clay) minerals (e.g., ferrihydrite, gibbsite and kaolinite) influence the isotope fractionation of Li during the adsorption and incorporation processes (Pistiner and Henderson, 2003). For example, an equilibrium fractionation factor [$\alpha = (^7Li/^6Li)_{mineral}/(^7Li/^6Li)_{fluid}$] of 0.971 (between secondary minerals and water) was observed when Li is adsorbed onto vermiculite (Zhang et al., 1998), a secondary mineral formed by altered biotite (Blum and Erel, 1997).

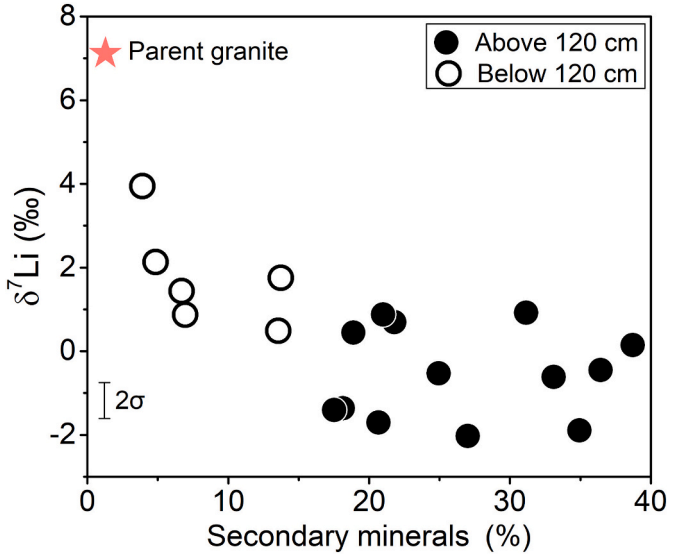

Fig. 6. δ^7Li values vs. secondary minerals (chlorite+vermiculite) along the weathering profile.

Thus, adsorption and/or incorporation of Li by secondary (or clay) minerals may be a significant cause of Li isotope fractionation in the study profile.

As discussed in Subsection 5.1.1, the successive weathering of biotite and plagioclase with different Sr isotope composition is responsible for the variation in $^{87}Sr/^{86}Sr$ ratio in the profile (Fig. 3D). However, this mechanism cannot explain the variation in δ^7Li value in the saprolites, because the released Li during weathering does not inherit the Li isotope signature of biotite (+5.8‰) and plagioclase (+5.9‰). Assuming that the dissolution of biotite has little Li isotope fractionation due to the small amount of secondary minerals formation at the incipient stage of weathering. Because of the lowest δ^7Li value in biotite among the primary minerals, it can be expected that the δ^7Li value of weathered residues would be higher than that of the parent granites (+7.1‰) and would be continuously increased as the biotite weathers. Similarly, the release of Li from plagioclase will also cause the increase of δ^7Li value in the sprolites. However, the opposite was true for the saprolite profile, in which the δ^7Li value is clearly declined and lowers than those in parent granite (Figs. 5B and 7A). Quartz has a higher δ^7Li value (+19.9‰) than other primary minerals, since to the heavy ^{7}Li prefers the high-energy bond in quartz associated with its lower coordination number sites (two- or fourfold sites) (Teng et al., 2006b). The variation of the proportion of quartz are generally <10% in the examined profile. Accordingly, the variation of δ^7Li value in saprolite caused by variation in quartz content was calculated to be within ±1‰. The results suggest that the differential weathering of primary minerals is not the major cause of the variation in Li isotope composition in the saprolites.

Could an alternative explanation be that non-stoichiometric dissolution of biotite is a major factor controlling the variation of δ^7Li in saprolite below 120 cm depth? In other words, could preferential release of relatively isotopically heavier Li in the incipient stage of non-stoichiometric dissolution of biotite could be the main reason for the low δ^7Li values in residual saprolites? Previous studies have shown that ^{6}Li is preferentially substituted in octahedral sites in clay minerals, which is a mechanism of Li fractionation during the secondary mineral adsorption process (Wimpenny et al., 2015; Hindshaw et al., 2019). The heterogeneous distribution of Li isotopes in gibbsite (and illite), i.e., the isotopically lighter Li composition in the octahedral layer and relatively heavier Li in interlayer can result in a difference of δ^7Li value reaching up to ~20‰ (Williams and Hervig, 2005; Vigier et al., 2008; Wimpenny et al., 2015). Similar to many clay minerals, biotite is a 2:1 phyllosilicate with a structure of octahedral sheet situated between tetrahedral sheets (Bisdom et al., 1982), and the heterogeneous distribution of B and Sr isotopic composition have been found between interlayer and structural sites (tetrahedral and octahedral layer) of biotite (Erel et al., 2004; Voinot et al., 2013). Thus, it can be logically speculated that Li isotopes in biotite may have a similar heterogeneous distribution that isotopically heavier Li composition in the interlayer and at the same time be isotopically lighter Li in the octahedral layer. Because of the interlayer cations in biotite are generally released more rapidly than the octahedral and the tetrahedral cations during leaching (Taylor et al., 2000; Voinot et al., 2013). Therefore, we speculated that relatively heavier Li in the interlayer sites is preferentially released from biotite at the beginning of granite weathering, leaving the residual Li in saprolite (or secondary minerals) relatively enriched in ^{6}Li. This speculation is supported by the values of δ^7Li and τ_{Li} decrease as the biotite content decrease in the saprolites (Fig. 8). Of course, this speculation needs to be further verified by experiments, such as observing the Li isotope composition changes in the case of non-congruent dissolution of biotite.

The Rayleigh fractionation model has been used to quantify Li isotope fractionation during Li's leaching from igneous rocks (e.g., basalt, diabase, and granite), and the results showed that most of

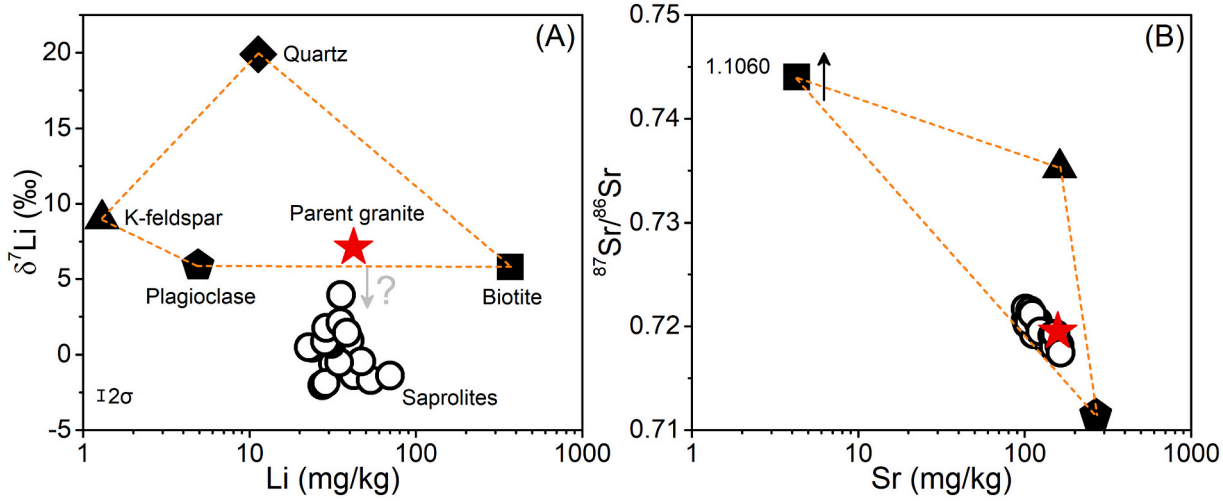

Fig. 7. Plot of δ^7Li vs. [Li] (mg/kg) (A) and $^{87}Sr/^{86}Sr$ vs. [Sr] (mg/kg) (B) in individual primary minerals, parent granite and saprolites. $^{87}Sr/^{86}Sr$ of biotite from White et al. (2001). The δ^7Li value in saprolites is lower than that in primary minerals. Does it indicate that Li isotope fractionation occurred during mineral decomposition?

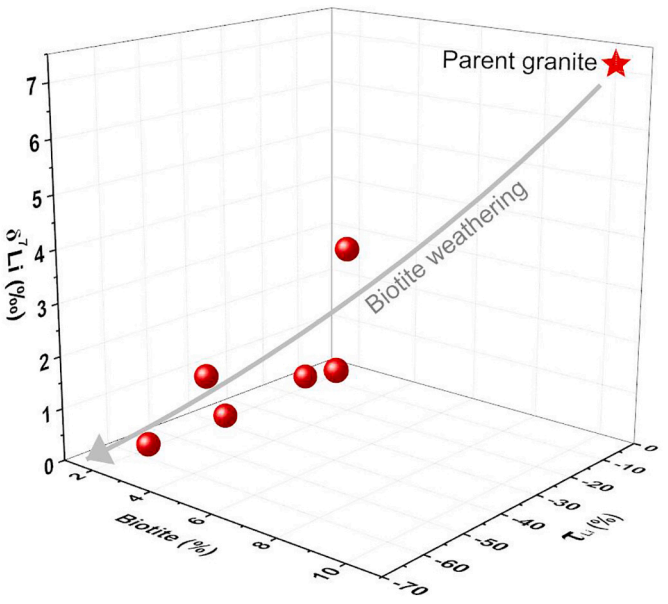

Fig. 8. The three-dimensional spatial relationship of biotite content, δ^7Li, and τ_{Li} in saprolites below 120 cm depth.

saprolites falls onto the Rayleigh distillation curves (Rudnick et al., 2004; Liu et al., 2013). However, a simple Rayleigh model assumes that the isotope compositions in the solid phase are well mixed and homogeneously released during weathering (e.g., Weiss et al., 2014). Therefore, this model cannot be used to quantify the Li isotope fractionation during weathering of biotite due to there may be heterogeneous distribution of Li isotope signatures between interlayer and structural sites of biotite.

5.3. Implications

The results of this study suggest that there is a significant Li isotope fractionation during the initial weathering of granite, in which ^{6}Li tends to remain in the weathering product, while ^{7}Li tends to be leached out. This corresponds to the high δ^7Li values found in the dissolved load of rivers flowing from relatively low weathering intensity catchments a granite (or gneiss) bedrock (Huh et al., 2001; Millot et al., 2010; Wimpenny et al., 2010a). Due to the smaller amounts of clay minerals formed in such catchments or in their weathering products, the clay mineralization cannot be the major factor responsible for Li isotope fractionation in such areas. Alternatively, the preferential uptake of ^{6}Li by newly formed Fe/Mn-oxyhydroxides may be the major cause(s) of the Li isotope fractionation in incipient weathering of rocks (Millot et al., 2010; Wimpenny et al., 2010a). It is also speculated in this study that the preferential release of ^{7}Li during non-stoichiometric dissolution of biotite (or other phyllosilicates) may be a further major contributor to Li isotope fractionation. Whatever the cause(s) of Li isotope fractionation, the fact is that Li released in the early stage of granite weathering has an obvious higher ^{7}Li/^{6}Li ratio than that of parent rock.

Certainly, many questions need to be clarified in future research. Previous studies have suggested that the mechanism of Li isotope fractionation during the adsorption of Li by clay minerals is a major controlling factor, however, the change in Li isotopic composition during the early dissolution of rock (or minerals) remains controversial. Experimental studies have also shown that there is almost no Li isotope fractionation at the initial stage of basalt and forsterite dissolution (Pistiner and Henderson, 2003; Wimpenny et al., 2010b). However, more recent data suggests that significant Li isotope fractionation occurs during the initial stage of basalt dissolution, possibly due to the rapid formation of clays that preferentially uptake ^{6}Li (Pogge von Strandmann et al., 2019). These Li isotope fractionation mechanisms may help to explain the effects of weathering regime, topography, and weathering intensity on variations of δ^7Li values in the dissolved load of rivers, and the relationship between tectonic uplift and increase marine ^{7}Li/^{6}Li ratios since the Cenozoic.

6. Conclusions

Lithium isotope behavior was carefully investigated in a saprolite profile with low weathering intensity developed on granite in the eastern Tibetan Plateau, China. Lithium concentration and isotopic composition in the primary minerals of granite are highly heterogeneous reflecting that Li is enriched in biotite while quartz contains the heavier Li isotope. Mineralogical composition and ^{87}Sr/^{86}Sr ratio measurements in the saprolites and parent granite suggest that biotite was preferentially weathered, followed by plagioclase. Lithium was distinctly lost during the weathering of biotite, and the values of δ^7Li in the saprolites were lower than that of parent granite, and gradually decreasing as weathering progresses. The variation of δ^7Li in the saprolite profile is not satisfactorily explained as being due to successive weathering of primary minerals. We speculate that Li isotope in biotite has a heterogeneous distribution in which the heavier ^{7}Li is preferentially released from the interlayer of biotite at the beginning of granite weathering, leaving the residual Li in the saprolites relatively enriched in ^{6}Li. If this is the case, Li isotope fractionation during weathering of granite is affected by adsorption and/or incorporation of Li by secondary minerals (or clay minerals) and the release of Li from biotite. Our results suggest that significant Li isotope fractionation occurs during the initial weathering of granite, which is consistent with the high δ^7Li values in the dissolved load in rivers from in low weathering intensity catchments and the lithology characteristic of granite (or gneiss). More efforts are needed to complement the mechanism of Li isotope fractionation during silicate weathering.

Declaration of Competing Interest

The authors declare that they have no known competing financial interests or personal relationships that could have appeared to influence the work reported in this paper.

Acknowledgments

We thank the Dr. He Hui-Jun (Ocean University of China) for help with separating Nd from saprolite and granite samples, and Dr. Olusegun K. Abass and Prof. Li Shao-Ming for help with writing skills and language polish. We would like to thank Dr. Paul Tomascak and Dr. Louis Derry for their valuable comments on the manuscript. We are especially grateful Dr. Philip A.E. Pogge von Strandmann and Dr. Xiao-Ming Liu and the editor Michael E. Böttcher for suggesting significant improvements to this manuscript. This work was supported jointly by the National Natural Science Foundation of China (No. 41930863, 42003007, 41661144042), and the Second Tibetan Plateau Scientific Expedition and Research (2019QZKK0707), and Special Fund for Basic Scientific Research of Central Colleges, Chang'an University (No. 3001102278302).

Appendix A. Supplementary data

Supplementary data to this article can be found online at https://doi.org/10.1016/j.chemgeo.2020.119969.

References

Berner, R.A., 1990. Atmospheric carbon-dioxide levels over phanerozoic time. Science 249, 1382–1386.

Bisdom, E.B.A., Stoops, G., Delvigne, J., Curmi, P., Altemuller, H.J., 1982. Micromorphology of weathering biotite and its secondary products. Pedologie 32 (2), 225–252.
Blum, J.D., Erel, Y., 1997. Rb-Sr isotope systematics of a granitic soil chronosequence: the importance of biotite weathering. Geochim. Cosmochim. Acta 61, 3193–3204.
Chadwick, O.A., Brimhall, G.H., Hendricks, D.M., 1990. From a black to a gray box—a mass balance interpretation of pedogenesis. Geomorphology 3 (3–4), 369–390.
Chan, L.H., Hein, J.R., 2007. Lithium contents and isotopic compositions of ferromanganese deposits from the global ocean. Deep Sea Res. II: Top. Stud. Oceanogr. 54 (11–13), 1147–1162.
Chauvel, C., Garçon, M., Bureau, S., Besnault, A., Jahn, B.M., Ding, Z., 2014. Constraints from loess on the Hf–Nd isotopic composition of the upper continental crust. Earth Planet. Sci. Lett. 388, 48–58.
Che, H., Zhang, J., Zhao, Z.Q., He, H.J., 2018. Measurement of Neodymium Isotope in Seawater and its significance in Mixing of Water Masses. Chin. J. Anal. Chem. 46 (09), 1393–1399 (In Chinese with English abstract).
Choi, M.S., Ryu, J.S., Park, H.Y., Lee, K.S., Kil, Y., Shin, H.S., 2013. Precise determination of the lithium isotope ratio in geological samples using MC-ICP-MS with cool plasma. J. Anal. At. Spectrom. 28 (4), 505–509.
Dellinger, M., Gaillardet, J., Bouchez, J., Calmels, D., Louvat, P., Dosseto, A., Gorge, C., Alanoca, L., Maurice, L., 2015. Riverine Li isotope fractionation in the Amazon River basin controlled by the weathering regimes. Geochim. Cosmochim. Acta 164, 71–93.
Erel, Y., Blum, J.D., Roueff, E., Ganor, J., 2004. Lead and strontium isotopes as monitors of experimental granitoid mineral dissolution. Geochim. Cosmochim. Acta 68, 4649–4663.
Gou, L.F., Jin, Z., Pogge von Strandmann, P.A.P., Li, G., Qu, Y.X., Xiao, J., Galy, Deng L., A., 2019. Li isotopes in the middle Yellow River: Seasonal variability, sources and fractionation. Geochim. Cosmochim. Acta 248, 88–108.
He, D.F., Zhu, W.G., Zhong, H., Ren, T., Bai, Z.J., Fan, H.P., 2013. Zircon U–Pb geochronology and elemental and Sr–Nd–Hf isotopic geochemistry of the Daocheng granitic pluton from the Yidun Arc, SW China. J. Asian Earth Sci. 67, 1–17.
Hindshaw, R.S., Tosca, R., Goût, T.L., Farnan, I., Tosca, N.J., Tipper, E.T., 2019. Experimental constraints on Li isotope fractionation during clay formation. Geochim. Cosmochim. Acta 250, 219–237.
Huh, Y., Chan, L.H., Zhang, L., Edmond, J.M., 1998. Lithium and its isotopes in major world rivers: implications for weathering and the oceanic budget. Geochim. Cosmochim. Acta 62 (12), 2039–2051.
Huh, Y., Chan, L.H., Edmond, J.M., 2001. Lithium isotopes as a probe of weathering processes: Orinoco River. Earth Planet. Sci. Lett. 194, 189–199.
Huh, Y., Chan, L.H., Chadwick, O.A., 2004. Behavior of lithium and its isotopes during weathering of Hawaiian basalt. Geochem. Geophys. Geosyst. 5 (9).
Kısakürek, B., Widdowson, M., James, R.H., 2004. Behaviour of Li isotopes during continental weathering: the Bidar laterite profile, India. Chem. Geol. 212, 27–44.
Kısakürek, B., James, R.H., Harris, N.B., 2005. Li and δ^7Li in Himalayan rivers: proxies for silicate weathering? Earth Planet. Sci. Lett. 237, 387–401.
Lemarchand, E., Chabaux, F., Vigier, N., Millot, R., Pierret, M.C., 2010. Lithium isotope systematics in a forested granitic catchment (Strengbach, Vosges Mountains, France). Geochim. Cosmochim. Acta 74, 4612–4628.
Li, J., Huang, X.L., Wei, G.J., Liu, Y., Ma, J.L., Han, L., He, P.L., 2018. Lithium isotope fractionation during magmatic differentiation and hydrothermal processes in rare-metal granites. Geochim. Cosmochim. Acta 240, 64–79.
Li, W., Liu, X.M., 2020. Experimental investigation of lithium isotope fractionation during kaolinite adsorption: implications for chemical weathering. Geochim. Cosmochim. Acta 284, 156–172.
Li, W., Liu, X.M., Chadwick, O.A., 2020. Lithium isotope behavior in Hawaiian regoliths: soil-atmosphere-biosphere exchanges. Geochim. Cosmochim. Acta 285, 175–192.
Lin, J., Liu, Y., Hu, Z., Yang, L., Chen, K., Chen, H., Zong, K., Gao, S., 2016. Accurate determination of lithium isotope ratios by MC-ICP-MS without strict matrix-matching by using a novel washing method. J. Anal. At. Spectrom. 31 (2), 390–397.
Liu, W., Liu, C., Brantley, S.L., Xu, Z., Zhao, T., Liu, T., Yu, C., Xue, D., Zhao, Z., Cui, L., Zhang, Z., Fan, B., Gu, X., 2016. Deep weathering along a granite ridgeline in a subtropical climate. Chem. Geol. 427, 17–34.
Liu, X.M., Rudnick, R.L., McDonough, W.F., Cummings, M.L., 2013. Influence of chemical weathering on the composition of the continental crust: Insights from Li and Nd isotopes in bauxite profiles developed on Columbia River Basalts. Geochim. Cosmochim. Acta 115, 73–91.
Ma, T., Weynell, M., Li, S.L., Liu, Y., Chetelat, B., Zhong, J., Xu, S., Liu, C.Q., 2020. Lithium isotope compositions of the Yangtze River headwaters: weathering in high-relief catchments. Geochim. Cosmochim. Acta 280, 46–65.
Ma, Y., Liu, C., 2001. Sr isotope evolution during chemical weathering of granites. Sci. China Ser. D Earth Sci. 44 (8), 726–734.
Maffre, P., Goddéris, Y., Vigier, N., Moquet, J.S., Carretier, S., 2020. Modelling the riverine δ^7Li variability throughout the Amazon Basin. Chem. Geol. 532, 119336.
Mao, H., Zhao, Z., Cui, L., Liu, C., 2018. The influence of climate and topography on chemical weathering of granitic regoliths in the monsoon region of China. Acta Geochim. 37 (5), 758–768.
Marschall, H.R., Wanless, V.D., Shimizu, N., Pogge von Strandmann, P.A.E., Elliott, T., Monteleone, B.D., 2017. The boron and lithium isotopic composition of mid-ocean ridge basalts and the mantle. Geochim. Cosmochim. Acta 207, 102–138.
Middelburg, J.J., van der Weijden, C.H., Woittiez, J.R., 1988. Chemical processes affecting the mobility of major, minor and trace elements during weathering of granitic rocks. Chem. Geol. 68 (3–4), 253–273.
Millot, R., Vigier, N., Gaillardet, J., 2010. Behaviour of lithium and its isotopes during weathering in the Mackenzie Basin, Canada. Geochim. Cosmochim. Acta 74, 3897–3912.
Murphy, M.J., Porcelli, D., Pogge von Strandmann, P.A.E., Hirst, C.A., Kutscher, L., Katchinoff, J.A., Mörth, C.M., Maximov, T., Andersson, P.S., 2019. Tracing silicate weathering processes in the permafrost-dominated Lena River watershed using lithium isotopes. Geochim. Cosmochim. Acta 245, 154–171.
Négrel, P., Millot, R., 2019. Behaviour of Li isotopes during regolith formation on granite (Massif Central, France): controls on the dissolved load in water, saprolite, soil and sediment. Chem. Geol. 523, 121–132.
Nesbitt, H., Young, G.M., 1982. Early Proterozoic climates and plate motions inferred from major element chemistry of lutites. Nature 299, 715.
Pistiner, J.S., Henderson, G.M., 2003. Lithium-isotope fractionation during continental weathering processes. Earth Planet. Sci. Lett. 214, 327–339.
Pogge von Strandmann, P.A.E., Henderson, G.M., 2015. The Li isotope response to mountain uplift. Geology 43 (1), 67–70.
Pogge von Strandmann, P.A.E., Frings, P.J., Murphy, M.J., 2017. Lithium isotope behaviour during weathering in the Ganges Alluvial Plain. Geochim. Cosmochim. Acta 198, 17–31.
Pogge von Strandmann, P.A.E., Fraser, W.T., Hammond, S.J., Tarbuck, G., Wood, I.G., Oelkers, E.H., Murphy, M.J., 2019. Experimental determination of Li isotope behaviour during basalt weathering. Chem. Geol. 517, 34–43.
Pogge von Strandmann, P.A.E., Kasemann, S.A., Wimpenny, J.B., 2020. Lithium and Lithium isotopes in earth's surface cycles. Elements Int. Magaz. Mineral. Geochem. Petrol. 16 (4), 253–258.
Raczek, I., Jochum, K.P., Hofmann, A.W., 2003. Neodymium and strontium isotope data for USGS reference materials BCR-1, BCR-2, BHVO-1, BHVO-2, AGV-1, AGV-2, GSP-1, GSP-2 and eight MPI-DING reference glasses. Geostand. Newslett. 27 (2), 173–179.
Rao, W., Chen, J.U.N., Yang, J., Ji, J., Li, G., Tan, H., 2008. Sr-Nd isotopic characteristics of eolian deposits in the Erdos Desert and Chinese Loess Plateau: Implications for their provenances. Geochem. J. 42 (3), 273–282.
Raymo, M.E., Ruddiman, W.F., 1992. Tectonic forcing of late Cenozoic climate. Nature 359, 117.
Romer, R.L., Meixner, A., Förster, H.J., 2014. Lithium and boron in late-orogenic granites–Isotopic fingerprints for the source of crustal melts? Geochim. Cosmochim. Acta 131, 98–114.
Rudnick, R.L., Tomascak, P.B., Njo, H.B., Gardner, L.R., 2004. Extreme lithium isotopic fractionation during continental weathering revealed in saprolites from South Carolina. Chem. Geol. 212, 45–57.
Ryu, J.S., Vigier, N., Lee, S.W., Lee, K.S., Chadwick, O.A., 2014. Variation of lithium isotope geochemistry during basalt weathering and secondary mineral transformations in Hawaii. Geochim. Cosmochim. Acta 145, 103–115.
Sauzéat, L., Rudnick, R.L., Chauvel, C., Garçon, M., Tang, M., 2015. New perspectives on the Li isotopic composition of the upper continental crust and its weathering signature. Earth Planet. Sci. Lett. 428, 181–192.
Schauble, E.A., 2004. Applying stable isotope fractionation theory to new systems. Rev. Mineral. Geochem. 55 (1), 65–111.
Sun, H., Gao, Y., Xiao, Y., Gu, H.O., Casey, J.F., 2016. Lithium isotope fractionation during incongruent melting: Constraints from post-collisional leucogranite and residual enclaves from Bengbu Uplift, China. Chem. Geol. 439, 71–82.
Taylor, A.S., Blum, J.D., Lasaga, A.C., MacInnis, I.N., 2000. Kinetics of dissolution and Sr release during biotite and phlogopite weathering. Geochim. Cosmochim. Acta 64, 1191–1208.
Teng, F.Z., McDonough, W.F., Rudnick, R.L., Walker, R.J., Sirbescu, M.L.C., 2006a. Lithium isotopic systematics of granites and pegmatites from the Black Hills, South Dakota. Am. Mineral. 91 (10), 1488–1498.
Teng, F.Z., McDonough, W.F., Rudnick, R.L., Walker, R.J., 2006b. Diffusion-driven extreme lithium isotopic fractionation in country rocks of the Tin Mountain pegmatite. Earth Planet. Sci. Lett. 243 (3–4), 701–710.
Teng, F.Z., Rudnick, R.L., McDonough, W.F., Wu, F.Y., 2009. Lithium isotopic systematics of A-type granites and their mafic enclaves: further constraints on the Li isotopic composition of the continental crust. Chem. Geol. 262, 370–379.
Vigier, N., Decarreau, A., Millot, R., Carignan, J., Petit, S., France-Lanord, C., 2008. Quantifying Li isotope fractionation during smectite formation and implications for the Li cycle. Geochim. Cosmochim. Acta 72 (3), 780–792.
Voinot, A., Lemarchand, D., Collignon, C., Granet, M., Chabaux, F., Turpault, M.P., 2013. Experimental dissolution vs. transformation of micas under acidic soil conditions: clues from boron isotopes. Geochim. Cosmochim. Acta 117, 144–160.
Wallmann, K., 2001. Controls on the cretaceous and Cenozoic evolution of seawater composition, atmospheric CO_2 and climate. Geochim. Cosmochim. Acta 65, 3005–3025.
Wang, Q.L., Chetelat, B., Zhao, Z.Q., Ding, H., Li, S.L., Wang, B.L., Li, J., Liu, X.L., 2015. Behavior of lithium isotopes in the Changjiang River system: sources effects and response to weathering and erosion. Geochim. Cosmochim. Acta 151, 117–132.
Weiss, D.J., Boye, K., Caldelas, C., Fendorf, S., 2014. Zinc isotope fractionation during early dissolution of biotite granite. Soil Sci. Soc. Am. J. 78 (1), 171–179.
White, A.F., Bullen, T.D., Schulz, M.S., Blum, A.E., Huntington, T.G., Peters, N.E., 2001. Differential rates of feldspar weathering in granitic regoliths. Geochim. Cosmochim. Acta 65, 847–869.
Williams, L.B., Hervig, R.L., 2005. Lithium and boron isotopes in illite-smectite: the importance of crystal size. Geochim. Cosmochim. Acta 69, 5705–5716.
Wimpenny, J., James, R.H., Burton, K.W., Gannoun, A., Mokadem, F., Gíslason, S.R., 2010a. Glacial effects on weathering processes: new insights from the elemental and lithium isotopic composition of West Greenland rivers. Earth Planet. Sci. Lett. 290, 427–437.
Wimpenny, J., Gíslason, S.R., James, R.H., Gannoun, A., Pogge von Strandmann, P.A.E., Burton, K.W., 2010b. The behaviour of Li and Mg isotopes during primary phase

dissolution and secondary mineral formation in basalt. Geochim. Cosmochim. Acta 74 (18), 5259–5279.
Wimpenny, J., Colla, C.A., Yu, P., Yin, Q.Z., Rustad, J.R., Casey, W.H., 2015. Lithium isotope fractionation during uptake by gibbsite. Geochim. Cosmochim. Acta 168, 133–150.
Yamaji, K., Makita, Y., Watanabe, H., Sonoda, A., Kanoh, H., Hirotsu, T., Ooi, K., 2001. Theoretical estimation of lithium isotopic reduced partition function ratio for lithium ions in aqueous solution. J. Phys. Chem. 105 (3), 602–613.
Yokoo, Y., Nakano, T., Nishikawa, M., Quan, H., 2004. Mineralogical variation of Sr–Nd isotopic and elemental compositions in loess and desert sand from the central Loess Plateau in China as a provenance tracer of wet and dry deposition in the northwestern Pacific. Chem. Geol. 204 (1–2), 45–62.
Zhang, J.W., Meng, J.L., Zhao, Z.Q., Liu, C.Q., 2019. Accurate Determination of Lithium Isotopic Compositions in Geological Samples by Multi-collector Inductively coupled Plasma-Mass Spectrometry. Chin. J. Anal. Chem. 47 (3), 415–422.
Zhang, L., Chan, L.H., Gieskes, J.M., 1998. Lithium isotope geochemistry of pore waters from Ocean Drilling Program Sites 918 and 919, Irminger Basin. Geochim. Cosmochim. Acta 62, 2437–2450.